

Dramatic bandwidth enhancement in nonlinear metastructures via bistable attachments

Cite as: Appl. Phys. Lett. 114, 093501 (2019); doi: 10.1063/1.5066329

Submitted: 14 October 2018 · Accepted: 17 February 2019 ·

Published Online: 5 March 2019



View Online



Export Citation



CrossMark

Yiwei Xia,¹ Massimo Ruzzene,^{1,2} and Alper Erturk^{1,a)}

AFFILIATIONS

¹G. W. Woodruff School of Mechanical Engineering, Georgia Institute of Technology, Atlanta, Georgia 30332, USA

²D. Guggenheim School of Aerospace Engineering, Georgia Institute of Technology, Atlanta, Georgia 30332, USA

^{a)}Author to whom correspondence should be addressed: alper.erturk@me.gatech.edu.

ABSTRACT

We report amplitude-dependent substantial enhancement of the frequency bandwidth in locally resonant metamaterial-based finite structures (metastructures) via bistable attachments. The bistable magnetoelastic beam attachments of the unit cells exhibit linear intrawell, nonlinear intrawell, and nonlinear interwell oscillations for low, moderate, and sufficiently high intensity excitations, respectively. As a result, the overall metastructure leverages linear locally resonant bandgaps under low amplitudes and nonlinear attenuation due to wideband chaotic vibrations of the bistable attachments under large amplitudes. The concept was first demonstrated through a linear mass-spring chain with bistable attachments in a numerical case study. Experimental results and validations are then presented for a base-excited cantilever beam hosting seven bistable unit cells. Transition from linear locally resonant bandgaps to nonlinear attenuation is observed, and the amplitude-dependent bandwidth enhancement is shown. The bandwidth offered by nonlinear interwell oscillations is substantially wider than the linear locally resonant bandgap that is limited by the added mass.

Published under license by AIP Publishing. <https://doi.org/10.1063/1.5066329>

Locally resonant linear metamaterials and the resulting finite metastructures with specified boundary conditions have been extensively studied in the past decade since the seminal work by Liu *et al.*¹ Elastic/acoustic metastructures made from locally resonant unit cells exhibit bandgaps at wavelengths much longer than the lattice size, enabling low-frequency vibration/noise attenuation and wave filtering, among other applications.^{1–7} In these linear locally resonant concepts, the bandgap size, i.e., the attenuation bandwidth, is limited by the added mass,⁷ which is to be minimized in most applications spanning from aerospace structures to those requiring compact designs due to space and other limitations.

Properly designed nonlinear oscillators offer various advantages, such as a substantially enhanced frequency bandwidth, as already leveraged in emerging fields such as vibration energy harvesting. For instance, monostable and bistable nonlinear oscillators have been employed to enable wideband energy harvesters over the past decade.⁸ Specifically, bistable configurations offer a plethora of wideband dynamics, such as periodic and chaotic interwell oscillations.^{9–11} These efforts shed light on the amplitude-dependent dynamics of an individual bistable oscillator for design (of the potential wells, etc.) to target a specific frequency bandwidth, not only in energy harvesting but also for other applications.

In terms of vibration attenuation using bistable attachments, researchers have mainly explored low degree-of-freedom (DOF) systems, rather than a metamaterial/metastructure setting. For example, Yang *et al.*¹² studied the steady-state response of a dual-stage system with a bistable first stage and a linear second stage under harmonic excitation. Manevitch *et al.*¹³ and Romeo *et al.*¹⁴ investigated, both analytically and numerically, the transient dissipative dynamics of a linear oscillator coupled with a bistable light attachment under impulse excitation in the context of passive nonlinear targeted energy transfer. Johnson *et al.*¹⁵ investigated vibration control using a bistable attachment from a disturbance cancellation perspective. These efforts unveil the potential of bistable attachments for wideband behavior although so far they have been limited to low DOF systems. It is worth mentioning that, in a parallel body of work, others^{16,17} have explored wave propagation in bistable lattices, demonstrating phenomena such as solitary wave propagation and unidirectional wave propagation.

This study explores amplitude-dependent bandwidth enhancement in locally resonant metamaterials/metastructures via bistable attachments. Specifically, it is of interest to leverage both the low amplitude linear locally resonant bandgap and the high amplitude wideband nonlinear attenuation. For the purpose of a basic qualitative concept demonstration, consider a linear mass-spring chain with

bistable attachments, as illustrated in Fig. 1. The system has $2N$ DOF with N identical main masses, m , and N identical bistable attachment masses, m_a . The main masses are connected to each other by identical linear springs of stiffness k , while the springs between the main masses and the attachments are nonlinear with a negative linear stiffness k_{a1} and a positive cubic stiffness k_{a3} . The potential energy of the i -th bistable attachment with respect to the corresponding main mass is $U_{ai} = k_{a1}x_{ai}^2/2 + k_{a3}x_{ai}^4/4$. Therefore, the attachments exhibit a double-well potential with two stable equilibrium positions as shown in Fig. 1. A harmonic external force $f(t) = f_1 \cos \Omega t$ is applied to the first main mass. The governing equations of motion for the i -th main mass and the i -th attachment are

$$(m + m_a)\ddot{x}_i + m_a\ddot{x}_{ai} - c\dot{x}_{i-1} + 2c\dot{x}_i - c\dot{x}_{i+1} - kx_{i-1} + 2kx_i - kx_{i+1} = f(t)\delta_{i1}, \quad (1)$$

$$m_a(\ddot{x}_i + \ddot{x}_{ai}) + c_a\dot{x}_{ai} + k_{a1}x_{ai} + k_{a3}x_{ai}^3 = 0, \quad (2)$$

where x_i is the absolute displacement of the i -th main mass, x_{ai} is the displacement of the i -th attachment relative to the i -th main mass, and δ_{ij} is the Kronecker delta. We nondimensionalize Eqs. (1) and (2), yielding

$$(1 + \mu)u_i'' + \mu u_{ai}'' - \zeta u_{i-1}' + 2\zeta u_i' - \zeta u_{i+1}' - u_{i-1}' + u_i + u_{i+1} = p\delta_{i1} \cos(\omega\tau), \quad (3)$$

$$u_i'' + u_{ai}'' + \zeta_a u_{ai}' + \alpha^2 u_{ai} + u_{ai}^3 = 0, \quad (4)$$

where the non-dimensional displacements are $u_i = x_i/L_c$ and $u_{ai} = x_{ai}/L_c$ (for the characteristic frequency $\Omega_c = \sqrt{k/m}$ and the characteristic length $L_c = \sqrt{m_a\Omega_c^2/k_{a3}}$). Furthermore, the non-dimensional time $\tau = \Omega_c t$, excitation frequency $\omega = \Omega/\Omega_c$, excitation amplitude $p = f/m\Omega_c^2 L_c$, mass ratio $\mu = m/m_a$, damping $\zeta = c/m\Omega_c$ and $\zeta_a = c_a/m_a\Omega_c$, and $\alpha^2 = k_{a1}/m_a\Omega_c^2$ are defined, while $(\cdot)'$ denotes the derivative with respect to non-dimensional time τ . With the choice of negative linear stiffness k_{a1} , α^2 is negative and there exist two stable equilibrium points for the attachment: $\bar{u}_{ai} = \pm\sqrt{-\alpha^2}$. Equation (4) can be linearized around either of the two stable equilibrium positions. The resulting linear natural frequency, β , of the

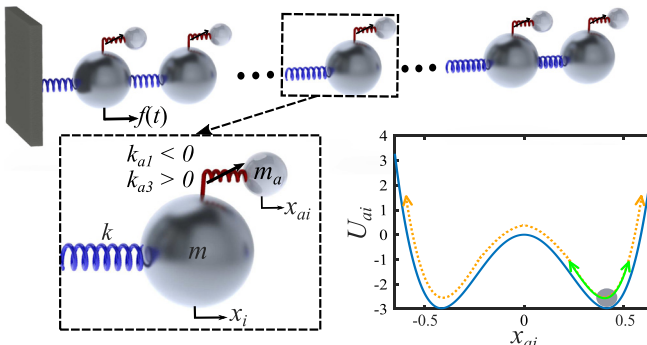


FIG. 1. Schematic of a linear mass-spring chain with bistable attachments showing an inset of a unit cell. The bottom right plot shows the double-well potential of i -th bistable attachment, U_{ai} , as a function of relative displacement x_{ai} , with illustrations of intrawell (green line) and interwell (orange dotted line) oscillations.

attachment around either of the two stable equilibrium positions is given by $\beta = \sqrt{-2\alpha^2}$.

For the nonlinear system in Fig. 1, response to harmonic excitation may exhibit periodic and aperiodic oscillations of intrawell and interwell types as known from the vast literature of bistable structures.^{8–11} For the periodic steady-state solutions of u_i and u_{ai} , the method of harmonic balance is used (more information on the harmonic balance method and its application examples for nonlinear structures can be found elsewhere^{18,19}). Since the system has cubic nonlinearities, the truncated Fourier series representation should contain sufficient terms;¹⁹ three harmonics are used here. The resulting nonlinear algebraic equations for the Fourier coefficients are then solved using the multivariate Newton-Raphson method. For aperiodic solutions (including chaos), the Runge-Kutta method (time-domain numerical simulation) is utilized.

The numerical case study considers a 10-DOF system, which includes 5 main masses and 5 bistable attachments. The following non-dimensional parameters are assumed: $\Omega_c = 1$, $L_c = \sqrt{5}$, $\mu = 0.1$, $\zeta = 0.1$, and $\zeta_a = 0.02$. In order to target the second mode of the plain mass-spring chain (for concept demonstration), the bistable attachments are tuned to have $\beta = \omega_{n2} = 0.8308$ (using $\alpha^2 = -0.3451$), where ω_{n2} is the second natural frequency of the 5-DOF plain mass-spring chain. Harmonic force is applied on the first main mass, and six levels of non-dimensional forcing amplitude are simulated. For the frequency response analysis of the nonlinear system, simulations are performed for both up and down frequency sweeps at each forcing amplitude over the non-dimensional frequency range of $0.6 < \omega < 1.1$.

Simulated non-dimensional results of frequency response (up and down sweep) for the 5-th mass are presented in Fig. 2 using the

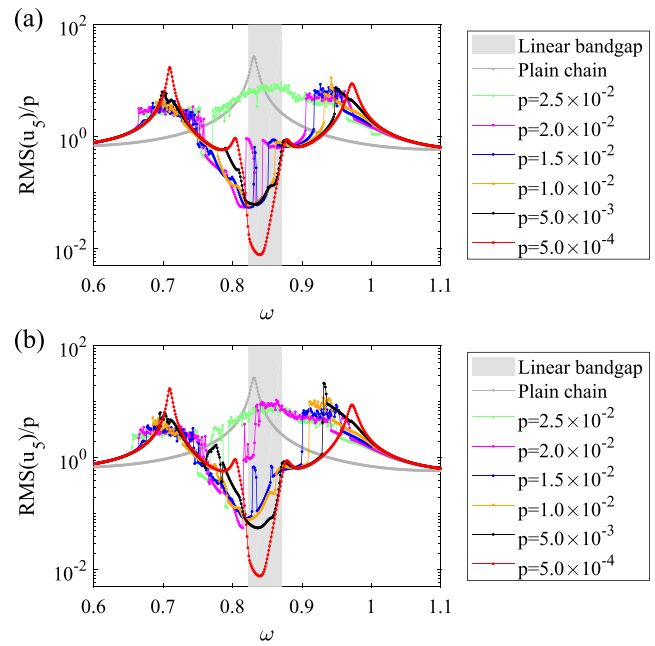


FIG. 2. Numerical simulation results for the non-dimensional displacement frequency response of the 5-th mass under different force levels normalized by the non-dimensional excitation amplitude: (a) up sweep and (b) down sweep.

root-mean-square (RMS) value at each frequency. For very low forcing levels (e.g., $p = 5.0 \times 10^{-4}$), the system exhibits linear/quasilinear behavior, yielding a locally resonant bandgap. The second mode (the target mode) of the plain mass-spring chain is attenuated while additional resonances appear, which is similar to the behavior of just using linear locally resonant attachments. The shaded region shows the linear bandgap based on the theory developed for a finite and discrete metamaterial chain.²⁰ As the forcing level increases, nonlinear introwell softening and interwell oscillations are enabled gradually. Specifically, interwell chaotic oscillations of the attachments yield a very broadband attenuation. For design and analysis purposes, it is of interest to quantify the level of forcing intensity required for escape from the potential wells of the bistable attachments. Here, a numerical analysis is performed to this end, as summarized next (analytical approaches exist for lower DOF systems²¹).

Figure 3 presents an example map for the prediction of the 5-th attachment's escape from the potential well by varying the forcing frequency and amplitude. The map is produced by varying the normalized frequency from 0.6 to 1.1 with increments of 5×10^{-4} , while varying the normalized forcing amplitude from 0 to 0.1 with steps of 5×10^{-4} . Both the black region and the yellow region represent introwell oscillations, with black denoting periodic oscillations using the harmonic balance method and yellow indicating aperiodic oscillations from time-domain simulations. Red regions represent the interwell chaotic oscillations of the attachments based on time-domain simulations. As can be seen from the map in Fig. 3, a threshold forcing amplitude exists for the bistable attachments to undergo introwell oscillations for all excitation frequencies. Remarkably, interwell oscillations are easier to form with a lower forcing amplitude especially around the two resonances of the linear/quasilinear frequency response curves (cf. the frequency axes in Figs. 2 and 3).

Experimental investigations are presented next to demonstrate the overall concept and validate amplitude-dependent bandwidth enhancement (Fig. 4). The metastructure is physically implemented in the form of a cantilever beam with 7 magnetoelastic beams as bistable local attachments. The experimental setup shown in Fig. 4 consists of a 3.175 mm thick, 3.175 cm wide, and 88.9 cm long aluminum beam, divided into 7 unit cells. The bistable attachments are made from spring steel cantilevers with tip masses. Two cube-shaped permanent magnets are placed at the tip of each spring steel cantilever. Each

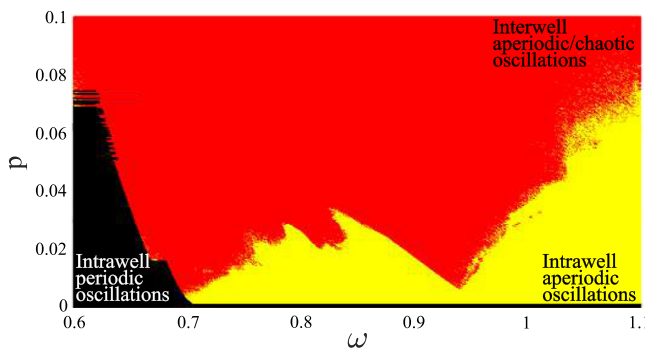


FIG. 3. Numerical map to quantify the forcing required for potential well escape of the 5-th attachment as a function of normalized frequency and normalized forcing amplitude.

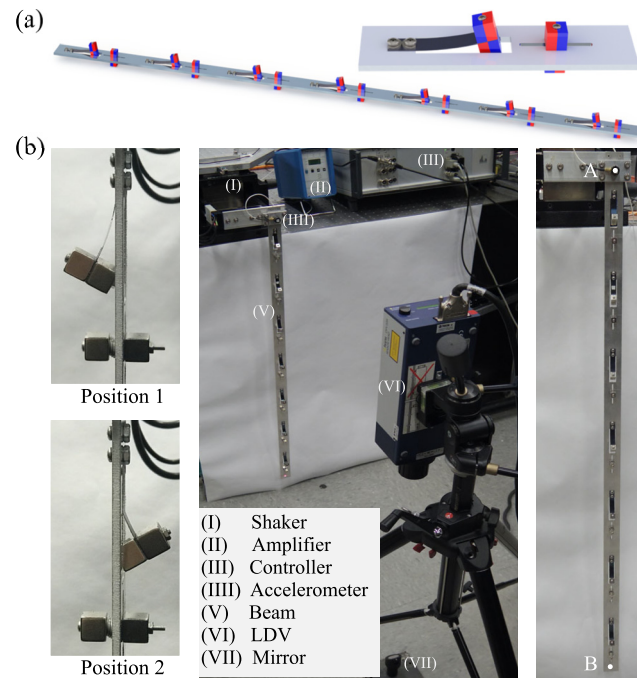


FIG. 4. (a) Metastructure (cantilevered beam with 7 magnetoelastic bistable beam attachments) with a close-up view of a unit cell (magnet polarity: red is north and blue is south). (b) Left: A bistable attachment in its two stable equilibrium positions. Middle: Experimental setup with an LDV oriented vertically at a 45° mirror to measure the transverse tip velocity of the beam. Right: Front view of the beam.

magnet has a hole through the center which is perpendicular to the magnetization direction. To realize the bistability, the other two magnets are attached on the aluminum beam [Fig. 4(a)] and two stable equilibrium positions are obtained [Fig. 4(b)]. Since the cantilever is clamped on one side of the aluminum beam, the thickness of the beam affects the symmetry of the double-well potential of the attachments. Spacers are placed between the beam and magnets to compensate for the beam thickness so that the double-well potential can be as symmetric as possible. The beam is clamped vertically to an APS-113 long stroke shaker, which excites the beam by base motion horizontally. The shaker is driven by an APS-125 amplifier and controlled by a SPEKTRA VSC-201 controller for the purpose of having a harmonic base acceleration at specified amplitudes and frequencies. Base acceleration measured using an accelerometer is fed back to the VSC-201 controller. The tip velocity of the beam is measured using a Polytec OFV-505 laser Doppler vibrometer (LDV) near the free end of the beam. The transmissibility frequency response of the beam is obtained by sweeping the excitation frequency up from 8 Hz to 20 Hz and down from 20 Hz to 8 Hz at a rate of 0.25 Hz/min for different base acceleration levels.

As shown in Fig. 5, the unit cells are designed to allow flexibility in the potential wells of the bistable attachments by varying the distance between magnets, which is quantified by the vertical distance, d , between the lower edge of the rectangular slot and the upper face of the cubic magnet. The transmissibility frequency response in Fig. 5(a) is defined as the ratio of the steady-state velocity at Point B to that at

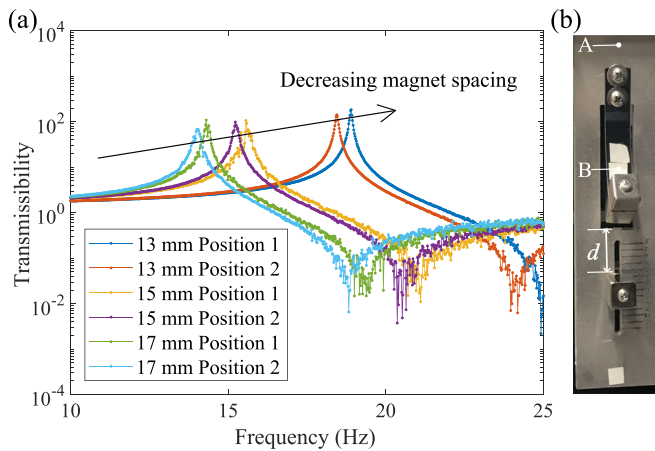


FIG. 5. (a) Effect of magnet spacing on the stable equilibrium positions of a bistable attachment (experimental) and (b) a close-up view.

Point A on the spring steel cantilever [shown in Fig. 5(b)]. Since the clamping of the spring steel cantilever is asymmetric, the resulting double-well potential is not perfectly symmetric in the experiments (i.e., a small amount of quadratic nonlinearity is inevitable). Slightly different post-buckled linear natural frequencies (previously defined as the non-dimensional β) are observed for the bistable attachment in stable equilibrium positions 1 and 2 (while it is negligible here, the effect of significantly asymmetric potential wells can be found in the nonlinear energy harvesting literature^{22,23}). As the distance between magnets decreases, the post-buckled linear natural frequency of the bistable attachment increases, which is a useful design and tuning parameter. With $d = 15$ mm, the post-buckled linear natural frequency is identified to be 15.1 Hz. This magnet spacing is selected to target the first mode neighborhood of the main structure in this work (as will be discussed next). Characterization of the unit cell with $d = 15$ mm is performed as shown in Fig. 6. As the base excitation level is increased, intrawell linear resonance turns into intrawell nonlinear softening, and then eventually interwell oscillations and chaos are observed with a substantial bandwidth, as expected from individual bistable beam dynamics.⁸

Having analyzed an individual unit cell in detail, experiments are performed on the main cantilevered structure with and without bistable attachments. In Fig. 7, the experimentally measured transmissibility frequency response of the beam under base excitation is plotted for various RMS base acceleration levels and for both up and down frequency sweep. Transmissibility here is defined as the ratio of the steady-state velocity at the tip of the aluminum beam [Point B in Fig. 4(b)] to that at its base [Point A in Fig. 4(b)]. The plain beam (baseline) here is the main cantilever without the bistable attachments, obtained by removing all 7 magnetoelastic cantilevers and the corresponding pairs of magnets at the tip, while keeping all other pairs of magnets on the beam with $d = 15$ mm. The first mode of the plain beam is identified to be at 16.14 Hz. The distance between the magnets can be tuned so that post-buckled linear resonance frequency of the bistable attachments is 16.14 Hz or higher. However, the higher post-buckled linear natural frequency is required, the shorter distance between the magnets is needed, and the deeper potential well is

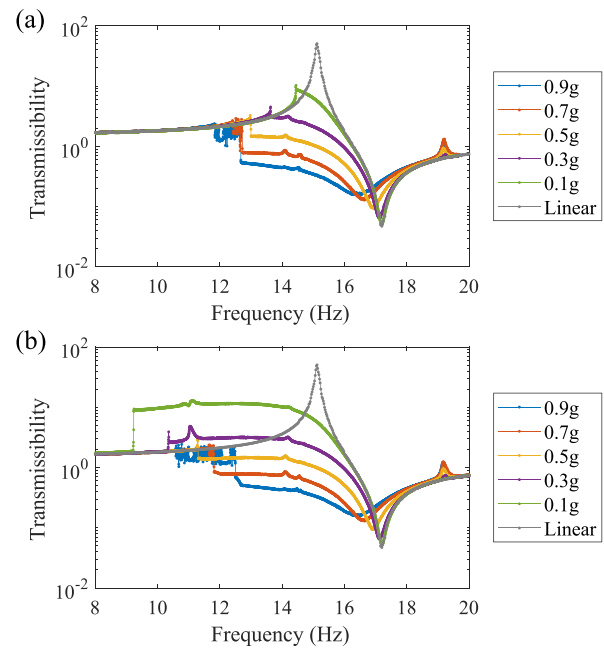


FIG. 6. Amplitude-dependent nonlinear characterization of a unit cell with magnet spacing $d = 15$ mm: (a) up sweep and (b) down sweep (experimental).

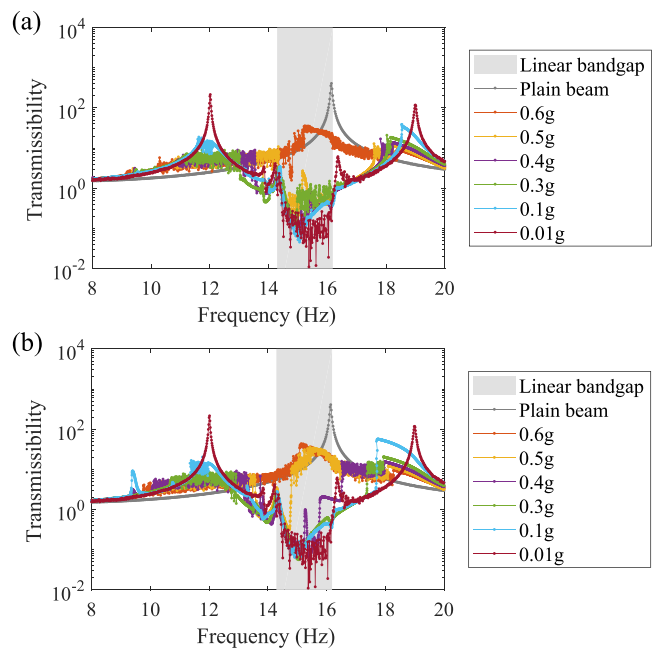


FIG. 7. Amplitude-dependent nonlinear dynamics of the metastructure with bistable attachments, showing a dramatic enhancement of the attenuation bandwidth (with comparisons against the plain beam and the locally resonant linear bandgap): (a) up sweep and (b) down sweep (experimental).

formed. In view of the experimental limitations (to avoid very deep potential wells and achieve escape from the potential wells for reasonable base excitation levels), $d = 15$ mm is deemed suitable to target the first mode neighborhood of the plain beam (cf. the frequency axes in Figs. 6 and 7). Note that variations in manually adjusted magnet spacing can lead to slightly different post-buckled linear natural frequencies for the bistable attachments. The post-buckled linear natural frequencies of all seven bistable attachments on the beam are identified individually, and the average value is 14.3 Hz. Even though the bistable attachments are not tuned to target the first mode of the beam exactly, the desired trends of vibration attenuation are kept, confirming the robustness of the nonlinear attenuation mechanism. At a very low RMS base acceleration level (0.01 g), it is observed that the bistable attachments remain within the potential well, vibrating linearly/quasi-linearly around their respective static equilibria. The metastructure experiences a bandgap similar to the one with linear local resonators, with the first mode of the plain beam attenuated while new resonances appear. The shaded region shows the linear locally resonant bandgap estimate based on the theory developed for finite and continuous metastructures,⁷ $\omega_l < \omega < \omega_t\sqrt{1 + \mu}$, with the target frequency $\omega_t = 14.3$ Hz and mass ratio $\mu = 0.27$. As the base excitation level increases, introwell softening of the resonators start triggering nonlinear attenuation first. Further increase in the base excitation intensity leads to a dramatic bandwidth enhancement (as compared to the linear bandgap) when interwell chaotic motions of the resonators are manifested.

In conclusion, we have investigated amplitude-dependent enhancement of the frequency bandwidth in locally resonant metastructures via bistable attachments, both numerically and experimentally. The bandwidth offered by nonlinear interwell oscillations of bistable attachments is substantially wider than the corresponding linear locally resonant bandgap. Such nonlinear vibrations can be triggered with the increasing excitation amplitude or by designing the potential wells (to be shallow enough) to ensure interwell dynamics for a given excitation level. This class of nonlinear metastructures

provide a much wider bandwidth than their linear counterparts whose bandgap is known to be limited by the added mass.

This work was supported by the Air Force Office of Scientific Research Grant No. FA9550-15-1-0397.

REFERENCES

- ¹Z. Liu, X. Zhang, Y. Mao, Y. Zhu, Z. Yang, C. T. Chan, and P. Sheng, *Science* **289**, 1734 (2000).
- ²D. Yu, Y. Liu, H. Zhao, G. Wang, and J. Qiu, *Phys. Rev. B* **73**, 064301 (2006).
- ³H. Sun, X. Du, and P. F. Pai, *J. Intell. Mater. Syst. Struct.* **21**, 1085 (2010).
- ⁴M. Oudich, M. Senesi, M. B. Assouar, M. Ruzzene, J.-H. Sun, B. Vincent, Z. Hou, and T.-T. Wu, *Phys. Rev. B* **84**, 165136 (2011).
- ⁵M. B. Assouar, M. Senesi, M. Oudich, M. Ruzzene, and Z. Hou, *Appl. Phys. Lett.* **101**, 173505 (2012).
- ⁶R. Zhu, X. Liu, G. Hu, C. Sun, and G. Huang, *J. Sound Vib.* **333**, 2759 (2014).
- ⁷C. Sugino, S. Leadenham, M. Ruzzene, and A. Erturk, *J. Appl. Phys.* **120**, 134501 (2016).
- ⁸M. F. Daqaq, R. Masana, A. Erturk, and D. D. Quinn, *Appl. Mech. Rev.* **66**, 040801 (2014).
- ⁹A. Erturk, J. Hoffmann, and D. Inman, *Appl. Phys. Lett.* **94**, 254102 (2009).
- ¹⁰F. Cottone, H. Vocca, and L. Gammaitoni, *Phys. Rev. Lett.* **102**, 080601 (2009).
- ¹¹S. C. Stanton, C. C. McGehee, and B. P. Mann, *Physica D* **239**, 640 (2010).
- ¹²K. Yang, R. Harne, K. Wang, and H. Huang, *Smart Mater. Struct.* **23**, 045033 (2014).
- ¹³L. I. Manevitch, G. Sigalov, F. Romeo, L. A. Bergman, and A. Vakakis, *J. Appl. Mech.* **81**, 041011 (2013).
- ¹⁴F. Romeo, G. Sigalov, L. A. Bergman, and A. F. Vakakis, *J. Comput. Nonlinear Dyn.* **10**, 011007 (2014).
- ¹⁵D. R. Johnson, R. Harne, and K. Wang, *J. Vib. Acoust.* **136**, 031006 (2014).
- ¹⁶N. Nadkarni, C. Daraio, and D. M. Kochmann, *Phys. Rev. E* **90**, 023204 (2014).
- ¹⁷N. Nadkarni, A. F. Arrieta, C. Chong, D. M. Kochmann, and C. Daraio, *Phys. Rev. Lett.* **116**, 244501 (2016).
- ¹⁸S. C. Stanton, B. A. Owens, and B. P. Mann, *J. Sound Vib.* **331**, 3617 (2012).
- ¹⁹S. Leadenham and A. Erturk, *Smart Mater. Struct.* **24**, 055021 (2015).
- ²⁰H. Al Ba'ba'a, M. Nouh, and T. Singh, *J. Sound Vib.* **410**, 429 (2017).
- ²¹L. N. Virgin, R. H. Plaut, and C.-C. Cheng, *Int. J. Non-linear Mech.* **27**, 357 (1992).
- ²²Q. He and M. F. Daqaq, *J. Sound Vib.* **333**, 3479 (2014).
- ²³W. Wang, J. Cao, C. R. Bowen, D. J. Inman, and J. Lin, *Appl. Phys. Lett.* **112**, 213903 (2018).